Factors that affect the intracellular localization and trafficking of African horse sickness virus core protein, VP7

Shani Bekker, Henk Huismans, Vida van Staden*

Department of Genetics, University of Pretoria, Pretoria 0002, South Africa

A B S T R A C T

African horse sickness virus (AHSV) VP7 is the major core protein of the virion. Apart from its role in virus assembly, VP7 forms crystalline-like particles during infection and when expressed in insect cells. The aim of this study was to investigate the process of VP7 crystalline-like particle formation. The intracellular distribution of VP7 was characterized in different systems and the association of VP7 with virus factories during AHSV infection was investigated. It was shown that the majority of VP7 is sequestered into these particles, and is therefore not available for new virion assembly. This is likely to have a negative impact on virus assembly and yield. By using specific markers and inhibitors of host trafficking pathways, VP7 localization was shown to be independent of host trafficking mechanisms and evaded host defenses against aggregation. Studying the process of VP7 crystalline-like particle formation will help us further understand AHSV replication and assembly.

Keywords:
AHSV
VP7
Virus factories
Host trafficking pathway
Microtubules
Aggresome
Proteasome
Ubiquitin
Lysosome

Introduction

African horse sickness (AHS) is a vector-borne disease of equids that can cause up to 90% mortality in susceptible horses and places a significant economic burden on equine industries due to a sanctioned restriction of movement of horses from affected areas (Mellor and Hamblin, 2004). The disease is endemic in sub-Saharan Africa, and is listed as a notifiable viral disease by the World Organization for Animal Health (OIE). AHS is caused by an orbivirus of the family *Reoviridae* known as African horse sickness virus (AHSV). The virus is transmitted by the biting midge, *Culicoides imicola*, and replicates efficiently in both insect and mammalian hosts (Du Toit, 1944; Venter et al., 2009). The AHSV virion is modelled after the orbivirus prototype, bluetongue virus (BTV) – a noneveloped virus composed of two layers of proteins that are organized into an outer capsid consisting of proteins VP2 and VP5, and an icosahedral core particle composed of major core proteins VP7 and VP3 (Hewat et al., 1992b). The core particle contains a genome of 10 segments of dsRNA and a transcription complex of three minor enzymatic proteins VP1, VP4, and VP6 (Grubman and Lewis, 1992; Roy et al., 1994). During infection the outer capsid proteins are responsible for entry into target cells, followed by the release of the core particle into the cytoplasm where it becomes transcriptionally active (Hassan et al., 2001; Hassan and Roy, 1999; Huismans et al., 1987; Huismans and Verwoerd, 1973). As infection progresses viral inclusion bodies (VIBs), directed by non-structural protein NS2, begin to form and act as sites for virus replication and early viral assembly (Brookes et al., 1993; Kar et al., 2007).

VP7 forms the outer layer of the virus core particle by assembling into trimers that attach perpendicularly to the interior VP3 surface of the subcore. Each VP7 monomer is composed of a top domain (formed by aa 121–249) and a bottom domain (made up of the N- and C-terminal regions, aa 1-120 and aa 250-349 respectively). The bottom domain of VP7 trimers make contact with the VP3 proteins, forming a precise VP7 lattice composed of 260 trimers that are deposited onto the inner VP3 scaffold that encloses the genome and transcription complex (subcore). This results in a stable icosahedral core particle (Basak et al., 1992; Grimes et al., 1995, 1997, 1998; Hewat et al., 1992a; Prasad et al., 1992). When the VP7 and VP3 genes are simultaneously expressed in a baculovirus expression system, the proteins spontaneously assemble into highly stable core-like particles (CLPs) (French and Roy, 1990; Maree et al., 1998). The expression of VP3 alone forms an unstable single-shelled subcore structure that can only be stabilized by the addition of VP7 (Le Blois and Roy, 1993; Limn

* Corresponding author. Tel.: +27 12 420 3257; fax: +27 12 362 5327.
E-mail address: vida.vanstaden@up.ac.za (V. van Staden).

and Roy, 2003; Limn et al., 2000). During virus assembly, the addition of the VP7 layer to the subcore is essential for the stabilization and protection of the newly packaged ssRNAs and is necessary prior to the trafficking of the assembled complex out of VIBs (Matsuo and Roy, 2013).

BTV VP7 has often been used as a model to experimentally describe intermolecular interactions in the BTV assembly process. However, very little is known about the process of AHSV core assembly. BTV and AHSV VP7 have 67% similarity (Roy et al., 1994) and are both able to spontaneously form soluble trimers when expressed in vitro (Basak et al., 1996; Limn et al., 2000; Rutkowska et al., 2011). Overall, the BTV VP7 protein is highly soluble and when expressed in isolation, it assembles into soluble trimers that are evenly distributed throughout the cell (Basak et al., 1996; Kar et al., 2007; Monastyrskaya et al., 1997; Oldfield et al., 1990). In contrast to BTV, the AHSV VP7 is said to be highly insoluble (Basak et al., 1996; Roy et al., 1991) and, unlike any of the cognate orbivirus proteins, forms unique flat hexagonal crystalline-like particles when expressed either in isolation in insect cells or in AHSV-infected cells (Burroughs et al., 1994; Chuma et al., 1992; Venter et al., 2012). The impact of the formation of these particles or their role during AHSV replication remains to be discovered. The formation of these crystalline-like particles appears to limit in vitro CLP formation by sequestering available soluble VP7 trimers and preventing them from incorporating onto the subcore (Maree et al., 1998). Given that the majority of soluble BTV VP7 is present in VIBs during core assembly, the sequestration of avail-able VP7 during AHSV core assembly will likely have a negative effect on the efficiency of AHSV core assembly and resulting viral yield.

In general, many viruses induce cellular remodelling during infection which results in the formation of similar insoluble aggregates that generally contain viral structural proteins. These aggregates are sometimes used by viruses to hold and accumulate large complexes of both viral and host proteins to protect and promote viral replication, assembly, and intracellular transportation (Kopito, 2000; Moshe and Gorovits, 2012; Wileman, 2006). Viruses often target and exploit key stages in host regulatory protein trafficking pathways, such as cytoskeleton or aggresomal pathways, as a means to move throughout the cytoplasm or to generate sites for virus replication (Dohner et al., 2005; Vogel et al., 2007). Viral factories, which are generally maintained by microtubules and localized near the microtubule organizing center (MTOC), often resemble aggresomes (Heath et al., 2001). Aggresomes are generally formed in response to cellular stress from protein aggregation or misfolding and hold aggregated proteins in a vimentin cage for subsequent proteasomal or autophagic degradation (Ciechanover, 2005; Kopito, 2000; Wileman, 2007). Thus the formation of these AHSV VP7 particles may, alternatively, result from activation of host defense mechanisms that recognize virus components and consequently sequester them into aggre-gates which are then targeted for storage and/or degradation.

Very little is known about the process of AHSV VP7 crystalline-like particle formation during virus infection, specifically whether the formation of these particles is caused by interaction with host cellular trafficking pathways or defenses against viral infection or, alternatively, whether these particles result from aggregation due to overexpression or misfolding. Here, we aim to investigate aspects associated with the formation of AHSV VP7 crystalline-like particles by studying VP7 intracellular distribution in different cell-types and expression systems. We also examine the role of host trafficking pathways and defense mechanisms in the formation of AHSV VP7 crystalline-particles. To support this study, we used an eGFP-tagged AHSV VP7 fusion protein, designated VP7-144-eGFP, to facilitate the tracking of the protein inside the cell. We could show that the VP7-144-eGFP fusion protein properly assembles into trimers and that the VP7-eGFP fusion protein resembles the intracellular distribution of wild-type VP7, allowing us to use it as a tool to study VP7 intracellular trafficking behaviour. We first examined and characterized the trafficking and intracellular distribution of VP7 in both insect and mamma-lian cells (transient expression), as well as in the presence of other AHSV proteins (i.e. in AHSV-infected cells). We also examined the association of VP7 with VIBs in AHSV-infected cells and found that crystalline-like particle formation is likely to have a negative impact on virus assembly. We then set out to determine if VP7 interacts with host trafficking pathways by examining the localization of VP7 by using the VP7-144-eGFP fusion protein in conjunction with a range of cellular markers. This was followed by the chemical inhibition of certain trafficking pathways to examine the effect on VP7 localization and crystalline particle formation. In this study we describe how VP7 is localized in a manner that is inherent to AHSV VP7 itself.

Results

Identification and characterization of wild-type AHSV VP7 and VP7-eGFP fusion protein intracellular distribution

In order to facilitate the appropriate tracking of VP7 in the cell, we investigated whether the top domain of VP7 could be modified with the insertion of a large foreign protein, eGFP. A VP7-eGFP fusion protein was constructed by inserting eGFP into a multiple cloning site in the top domain of an available AHSV VP7 vector (Rutkowska et al., 2011) at amino acid position 144. The resulting VP7-eGFP fusion protein, VP7-144-eGFP, was then expressed in insect cells (Sf9 cells) using the baculovirus protein expression system. Protein synthesis was confirmed by SDS-PAGE and Western blot analysis using anti-VP7 antibody. The size of VP7-144-eGFP corresponded to the expected size of 68 kDa, and migrated slower than the 38 kDa wild-type VP7 protein (Fig. 1A and B, Lanes 3 and 4). To determine whether the insertion of eGFP into the VP7 top domain disrupted VP7 assembly and stability, we investigated its ability to form trimers by means of a modified SDS-PAGE analysis of unboiled samples previously described for the detection of VP7 trimers (Monastyrskaya et al., 1997). As shown in Fig. 1A and B, the 114 kDa wild-type VP7 and 204 kDa VP7-144-eGFP multimers migrated at a slower rate than their respective 38 and 68 kDa monomeric (M) counterparts when incubated at room temperature (RT). The presence of the high molecular weight trimer protein bands (T) in both wild-type and fusion VP7 protein samples confirmed that VP7-144-eGFP forms trimers, similar to wild-type VP7.

To establish the use of VP7-144-eGFP as an accurate marker for the investigation of the intracellular distribution of AHSV VP7, we compared the intracellular localization of VP7-144-eGFP in Sf9 cells to the localization of wild-type AHSV VP7 in recombinant baculovirus-infected Sf9 cells and AHSV-infected BSR cells. AHSV-infected BSR cells as well as Sf9 cells infected with recombinant baculovirus expressing wild-type AHSV VP7 were fixed at 48 h post infection (p.i.) and immunostained with antibody against AHSV VP7. Sf9 cells were also infected with recombinant baculo-virus expressing the VP7-144-eGFP fusion protein and its distribu-tion was detected following fixation by eGFP auto-fluorescence at 48 h p.i. using confocal microscopy (Fig. 2).

In the presence of other AHSV proteins in AHSV-infected cells (Fig. 2A), some VP7 localized to small punctate areas within the cytoplasm, however the majority of VP7 was concentrated as one distinct flat crystalline-like particle within each cell. In Sf9 cells, both the recombinant baculovirus-expressed wild-type AHSV VP7 (Fig. 2B) and VP7-144-eGFP fusion protein (Fig. 2C) formed small

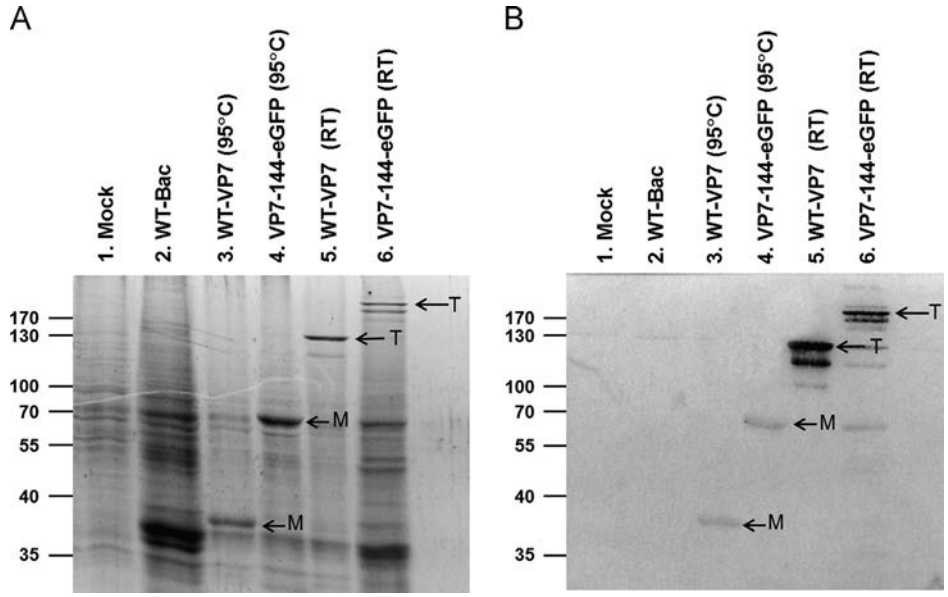

Fig. 1. Expression and trimerization assay of wild-type (WT) VP7 and VP7-144-eGFP proteins. Sf9 cells were infected with recombinant baculovirus expressing either WT-VP7 or VP7-144-eGFP. Cells were harvested at 48 h p.i., lysed, and assayed for trimer formation. Coomassie blue-stained SDS-PAGE (A) and Western blot using anti-VP7 antibodies (B) profiles of boiled (95 °C) and unboiled (RT) VP7 samples. The WT and fusion proteins are indicated. The positions of VP7 monomers (M) and trimers (T) are indicated. The doublets observed in lanes 5 and 6 indicate the instability of trimers in the presence of SDS at RT.

punctate foci in the cytoplasm as well as a single, highly localized structure within the cell. Upon three-dimensional reconstruction (rendered z-stack analysis) using Zeiss LSM imaging software, the structures formed by wild-type VP7 in Sf9 cells were found to be flat crystalline-like structures with a similar morphology to those seen in AHSV-infected cells (Fig. 2B). Similarly, the foci formed by VP7-144-eGFP in Sf9 cells were found to be flat rigid structures (Fig. 2C) comparable to wild-type AHSV VP7. In all instances, the crystalline structures formed by the VP7 proteins appeared to range in size from 2 μm to 5 μm as previously reported for the ultrastructure of AHSV VP7 (Venter et al., 2014). The three-dimensional stacking results from Fig. 2B (right) show that the rectangular VP7 crystalline structures observed in Sf9 cells by confocal microscopy (Fig. 2B) and in AHSV-infected cells previously observed by transmission electron microscopy (Venter et al., 2014) represent the hexagonal AHSV VP7 crystals formerly isolated from AHSV-infected cells (Burroughs et al., 1994). In addition, these results indicate that VP7-144-eGFP fusion protein has a similar intracellular localization to wild-type VP7, and forms structures that represent a similar VP7 organization as the crystalline-like structures of wild-type VP7.

Next, we investigated if the VP7 incorporated into the crystalline-like particles co-localized with NS2, a marker for VIBs (Kar et al., 2007). AHSV-infected BSR cells were fixed and co-labeled with anti-NS2 and anti-VP7 antibodies at various times post infection (Fig. 3). The VP7 incorporated in the crystalline-like particles (boxes) was not associated with VIBs, while the VP7 in the smaller punctate foci (arrows) was associated with VIBs (Fig. 3). The small foci therefore represent the relatively minor amount of VP7 that is available for core particle formation during progeny virion assembly in the VIBs, while the majority of VP7 is packaged into crystalline-like particles and remains as crystalline-like particles over time.

To determine whether the recombinant VP7-eGFP fusion protein behaves similarly to wild-type VP7, we investigated the localization of VP7-144-eGFP relative to VIBs and compared it to the localization of wild-type AHSV VP7 relative to VIBs in Sf9 cells, in the absence of the majority of the other AHSV proteins. It has previously been suggested that VP3 is required to recruit VP7 to VIBs during BTV core assembly (Kar et al., 2007). We therefore included VP3 in these experiments. Sf9 cells were co-infected with recombinant baculoviruses expressing AHSV VP7, NS2, and VP3 (Fig. 4A) or VP7-144-eGFP, NS2, and VP3 (Fig. 4B). Cells were incubated for 48 h, fixed and VIBs were labeled with anti-NS2 and processed for immunofluorescence microscopy. In the case of cells expressing wild-type AHSV VP7, VP7 was labeled with anti-VP7 primary antibodies while the localization of VP7-144-eGFP was visualized based on eGFP auto-fluorescence. VP3 expression was confirmed separately by labeling Sf9 cells infected with recombinant baculovirus expressing VP3 with anti-VP3 primary antibody at 48 h p.i. (data not shown). Results show that the large structures formed by VP7-144-eGFP (boxes) do not localize with NS2, while the smaller more diffuse concentrations of VP7-144-eGFP (arrows) co-localized with the punctate foci of NS2 (VIBs) (Fig. 4B). A similar pattern was observed in Sf9 cells expressing wild-type AHSV VP7 and NS2 where the crystalline-like VP7 particles (boxes) were not associated with VIBs, while the smaller foci (arrows) localized with VIBs (Fig. 4A). The behaviour of VP7-144-eGFP is therefore similar to wild-type AHSV VP7 in AHSV-infected cells (Fig. 3) and in Sf9 cells expressing wild-type AHSV VP7 and NS2.

Together, these results indicate that the insertion of eGFP in the top domain of VP7 did not substantially affect the normal targeting, localization, or behaviour of AHSV VP7. VP7-144-eGFP could therefore be used as a tool to study AHSV VP7 trafficking in the cell.

Comparison of the intracellular distribution and trafficking of fusion protein VP7-144-eGFP in insect and mammalian cells

To gain a better understanding of the manner in which VP7 is trafficked to form these crystalline-like particles, we compared the intracellular distribution of baculovirus expressed VP7-144-eGFP in insect cells to that of transiently expressed VP7-144-eGFP in mammalian cells at various times. This would enable us to determine if the distribution of AHSV VP7 is cell-type specific, and to establish whether the high level of protein expression inherent to baculovirus expression systems in insect cells affects the normal localization and trafficking of VP7. To transiently

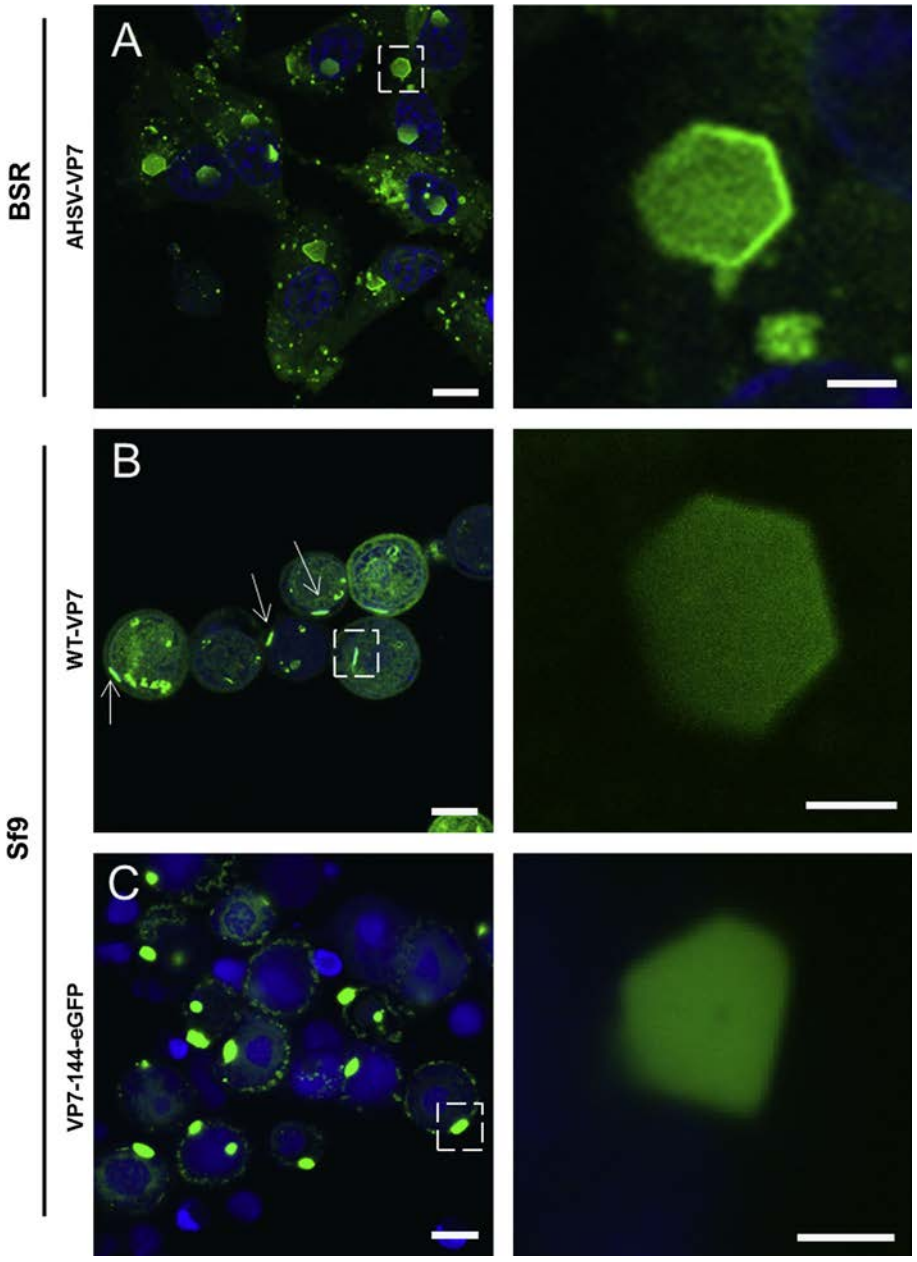

Fig. 2. Intracellular distribution of VP7 within AHSV- and recombinant baculovirus infected cells by confocal microscopy. (A) BSR cells infected with AHSV-4 and fixed at 48 h p.i. Magnified hexagonal VP7 crystalline-like particle is depicted on the right. (B) Sf9 cells infected with recombinant baculovirus expressing wild-type AHSV VP7 and fixed at 48 h p.i. Magnified three-dimensional reconstruction (rendered z-stack analysis) of crystalline-like particles (arrows) is shown on the right. (C) Sf9 cells infected with recombinant baculovirus expressing fusion protein VP7-144-eGFP, fixed at 48 h p.i. with refined and magnified image to the right. VP7 in A-B was detected with anti-VP7 antibody (guinea pig) and FITC conjugated secondary antibody (green). VP7 in C was visualized based on eGFP auto-fluorescence. Nuclei were stained with DAPI (blue). Scale bars represent 10 μm (panels to the left) and 2 μm in magnified images (panels to the right).

express the VP7-144-eGFP fusion protein in mammalian cells, the VP7-144-eGFP gene was cloned into a mammalian expression vector. Plasmid containing the VP7 fusion protein was then transfected into BSR cells using Lipofectamine2000 (Life Technologies) until the optimal concentration (0.8 μg) was determined by analysis of auto-fluorescence in live cells using confocal microscopy.

The distribution of VP7 over time was examined and compared in both insect and mammalian cells. Sf9 cells were infected with recombinant baculovirus expressing VP7-144-eGFP, and BSR cells were transfected with plasmid expressing VP7-144-eGFP fusion protein. Cells were incubated and visualized by immunofluorescence microscopy (fixed or unfixed) at a variety of times (ranging from 12 h to 72 h) post infection (p.i.) or post transfection (p.t.) to determine the kinetics of protein expression for each system (Fig. 5). The protein was initially homogenously distributed throughout the cytoplasm in both insect and mammalian cells (24 h p.i. and 36 h p.t. respectively), after which the VP7 distribu-tion became less diffuse and organized into multiple foci through-out the cytoplasm. As time progressed, the foci became less numerous and grew in size, after which they coalesced to one site alongside the nucleus to finally form the characteristic VP7 crystalline-like particle (48 h p.i. and 68 h p.t.). This intracellular distribution was not observed when eGFP was expressed alone, as eGFP was evenly distributed throughout the cell from 12 to 72 h
p.i./p.t. in both Sf9 and BSR cells (data not shown). To eliminate

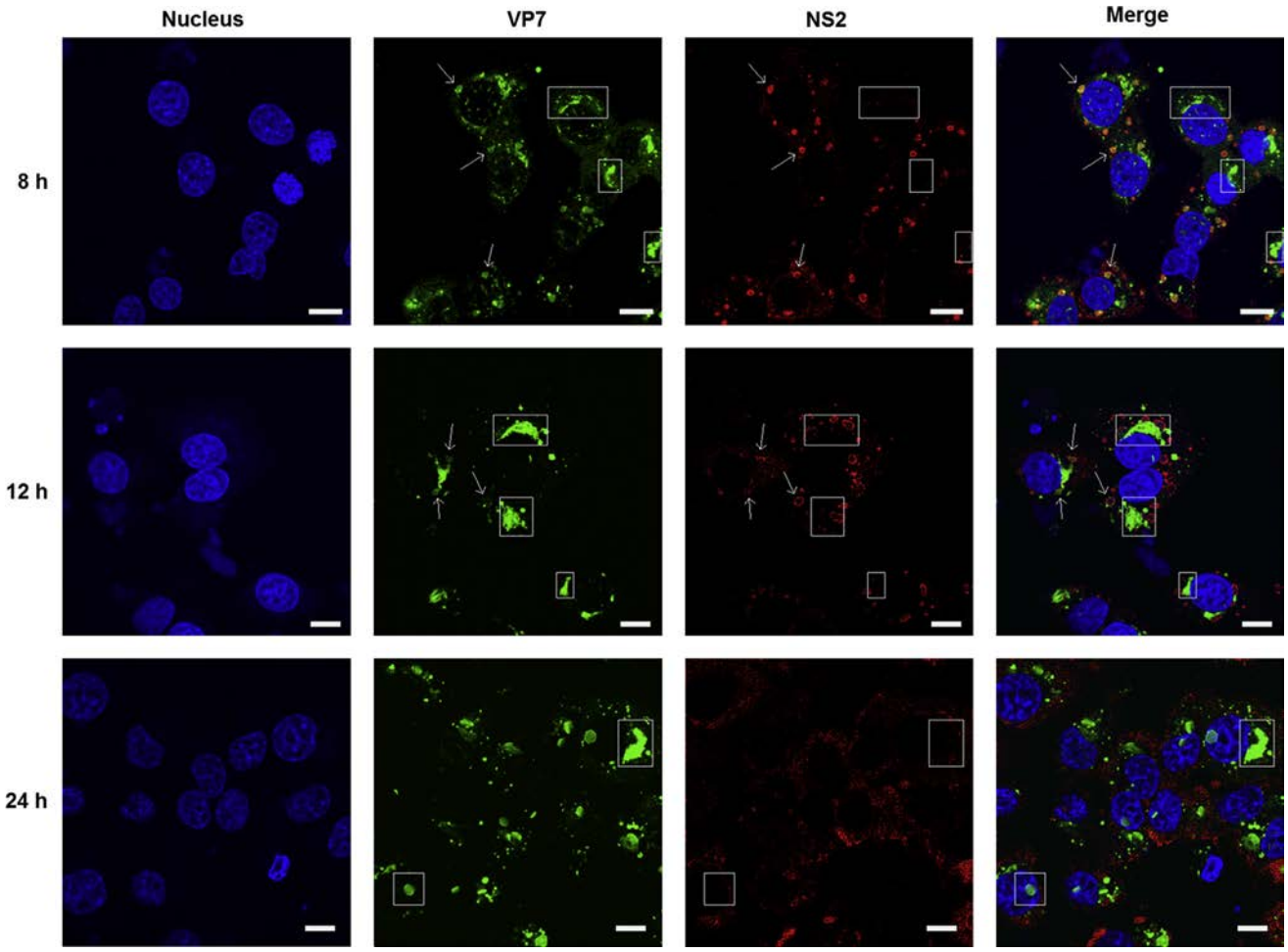

Fig. 3. Association of VP7 foci and crystalline-like particles with VIBs in AHSV-infected BSR cells at various times post infection by confocal microscopy. BSR cells were infected with AHSV-4 and fixed at 8 h, 12 h, and 24 h p.i. VP7 was detected with anti-VP7 primary antibody (guinea pig) and FITC conjugated secondary antibody (green), NS2 was detected with anti-NS2 primary antibody (rabbit) and Alexa Fluor 633 conjugated goat anti-rabbit secondary antibody (red). Nuclei were stained with DAPI (blue). Scale bars represent 10 μm.

artefacts that might arise from fixation of cells, unfixed live cells were also examined and similar fluorescent signals were visible in both insect and mammalian cells (Fig. 5 A and B bottom panels).

The data obtained thus far confirmed that the ability of VP7 to assemble into these large particles was not dependent on cell-type specific factors, since similar VP7 particles and intracellular distribution were observed in both insect and mammalian cells when VP7 was expressed by different systems (AHSV infection, recombinant baculovirus infection, and plasmid transfection). In addition, the diffuse distribution of VP7 at early times post infection indicated that AHSV VP7 was in fact expressed as a soluble protein, after which the protein was transported in the cell to coalesce and form an insoluble crystalline particle.

AHSV VP7 intracellular distribution and trafficking is not dependent on general host cell transport or defense mechanisms

We subsequently set out to determine if the crystalline structures formed by AHSV VP7 in infected and transfected cells coalesce as a result of interaction with host trafficking pathways and defense mechanisms. In each experiment, recombinant baculovirus-infected Sf9 cells expressing VP7-144-eGFP or BSR cells transfected with plasmid expressing VP7-144-eGFP were labeled with antibodies against specific cellular components in the presence or absence of the corresponding cellular transport-inhibiting drug. Cells were examined at times of active VP7 transport to multiple foci (24 h p.i. or 48 h p.t.) as well as at times of large crystalline-like particle formation (48 h p.i. or 68 h p.t.). The effects of the drug on the evolution and intracellular localization of VP7 particles was then visualized using confocal microscopy.

VP7 crystalline-like particle formation is not dependent on the microtubule network

To investigate the role of the microtubule network on the migration of VP7, cells were treated or not with colchicine, a microtubule depolymerizing drug, and subsequently labeled with anti-tubulin antibody. In pilot experiments using tubulin staining, we found that treatment of cells with colchicine at a concentration of 10 μM was sufficient to depolymerize the cellular microtubules. Cells expressing VP7-144-eGFP were treated or not with colchicine from the beginning of infection or transfection to time of fixation. Comparison of the untreated and treated cells (Fig. 6) showed that in spite of the microtubules being completely depolymerized at key points during expression, this did not cause a significant change in the size, morphology, intracellular distribution, or migration of VP7 in insect or mammalian cells (Fig. 6 bottom panel). These results established that VP7 foci are not positioned at the MTOC, and that transport along microtubules is not required for the formation of VP7 particles.

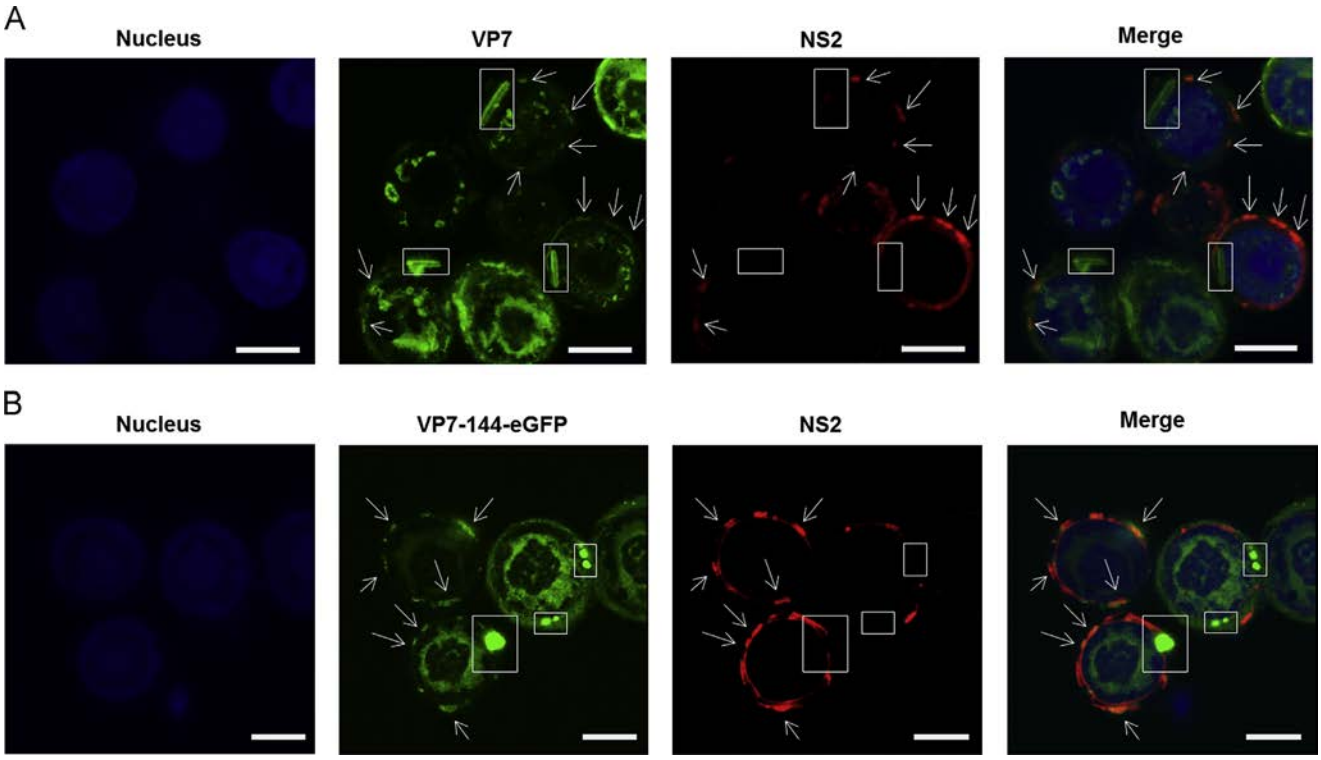

Fig. 4. Association of wild-type VP7 and VP7-144-eGFP with NS2 in the presence of VP3 in Sf9 cells. (A) Sf9 cells were co-infected with recombinant baculoviruses expressing AHSV NS2, VP3, and wild-type VP7 (A) or NS2, VP3 and VP7-144-eGFP (B) at a MOI of 10. Cells were fixed at 48 h p.i. and labeled with anti-NS2 antibody (rabbit) and Alexa Fluor 633 conjugated anti-rabbit secondary antibody (red). (A) VP7 was detected with anti-VP7 (guinea pig) primary antibody and FITC conjugated secondary antibody (green). (B) VP7-144-eGFP was visualized based on eGFP auto-fluorescence. Nuclei were stained with DAPI (blue). Scale bars represent 10 μm.

VP7 is not contained within or associated with the aggresomal pathway

Next, we sought to determine if the particles formed by VP7 in cells expressing VP7-144-eGFP were associated with aggresomes. Since aggresomes induce the redistribution of vimentin to form a cage-like structure around the aggregated protein, we labeled vimentin in order to determine if VP7 was contained within an aggresome. BSR cells were transfected with plasmid expressing VP7-144-eGFP and labeled with anti-vimentin. Labeling in Sf9 cells was not possible as antibodies for insect cell vimentin are unavailable. Results from Fig. 7A illustrate that vimentin is not redistributed to form a cage around the VP7 structure, and VP7 does not associate with vimentin. To confirm this finding, vimentin was disrupted in both recombinant baculovirus-infected Sf9 and transfected BSR cells using acrylamide (ACR), a drug that specifically disrupts the vimentin intermediate filament network (Fig. 7A and B) (Bhattacharya et al., 2007). In preliminary experiments cells were treated at various times and with various concentrations of ACR in order to obtain viable cells that had disrupted vimentin (confirmed by vimentin-labeling of treated cells). Cells were treated with 5 mM ACR at 24 h prior to fixation, as well as for the full period following infection or transfection. The disruption of vimentin did not have an effect on VP7 intracellular distribution in BSR (Fig. 7A bottom panel) and Sf9 cells (Fig. 7B). Aggresomes are commonly known to recruit misfolded proteins by the enzyme, Histone Deacetylase 6 (HDA6)(Kawaguchi et al., 2003). In order to determine if VP7 is misfolded in any way, cells were treated with Scriptaid, a Histone deacetylase 6 inhibitor. If VP7 is misfolded and targeted for aggresome formation, the inhibition of HDA6 would have an effect on the trafficking behaviour and the subsequent subcellular localization of VP7. Cells expressing VP7-144-eGFP were incubated in the presence of 5 μM Scriptaid according to conditions established previously (Beaudoin et al., 2008) and fixed at 48 h p.i. Results showed that the inhibition of HDAC 6 had no effect on VP7 trafficking or intracellular distribution (Fig. 7B). The same results were observed when transfected BSR cells expressing VP7-144-eGFP were treated with 5 μM Scriptaid (data not shown). These data and the lack of vimentin redistribution suggest that the particles formed by VP7-144-eGFP are not misfolded aggregates, and are not contained within an aggresome.

VP7 is not targeted for degradation by the host cell

When a foreign protein is expressed in a cell, that protein is often targeted for degradation by the ubiquitin–proteasome system (UPS) or the lysosomal pathway. In order to investigate the potential role of the UPS in VP7 distribution and crystalline-like particle formation, the 26 S proteasome as well as ubiquitin were stained and their association with VP7-144-eGFP was examined in insect and mammalian cells using confocal microscopy (Figs. 8 and 9). Results show that the large VP7 foci were not made up of ubiquinated protein (Figs. 8 and 9A), and do not co-localize with the proteasome (Figs. 8 and 9A). To confirm that VP7 was not associated with the proteasome, MG132 (a potent proteasome inhibitor) was also used. After treatment with a range of MG132 concentrations, both baculovirus-infected Sf9 and transfected BSR cells were treated with 100 μM of MG132 at 24 h p.i. or p.t. for optimal proteasomal inhibition. When the proteasome was inhibited, VP7 foci formation was not affected in either Sf9 or BSR cells (Figs. 8 and 9C). These results confirm that VP7 is not associated with the UPS.

The association of VP7 with lysosomes was examined by labeling lysosomes in Sf9 and BSR cells expressing VP7-144-eGFP using Lysotracker Red Dye (Life Technologies). There was no association of VP7 foci with the lysosome in either cell type

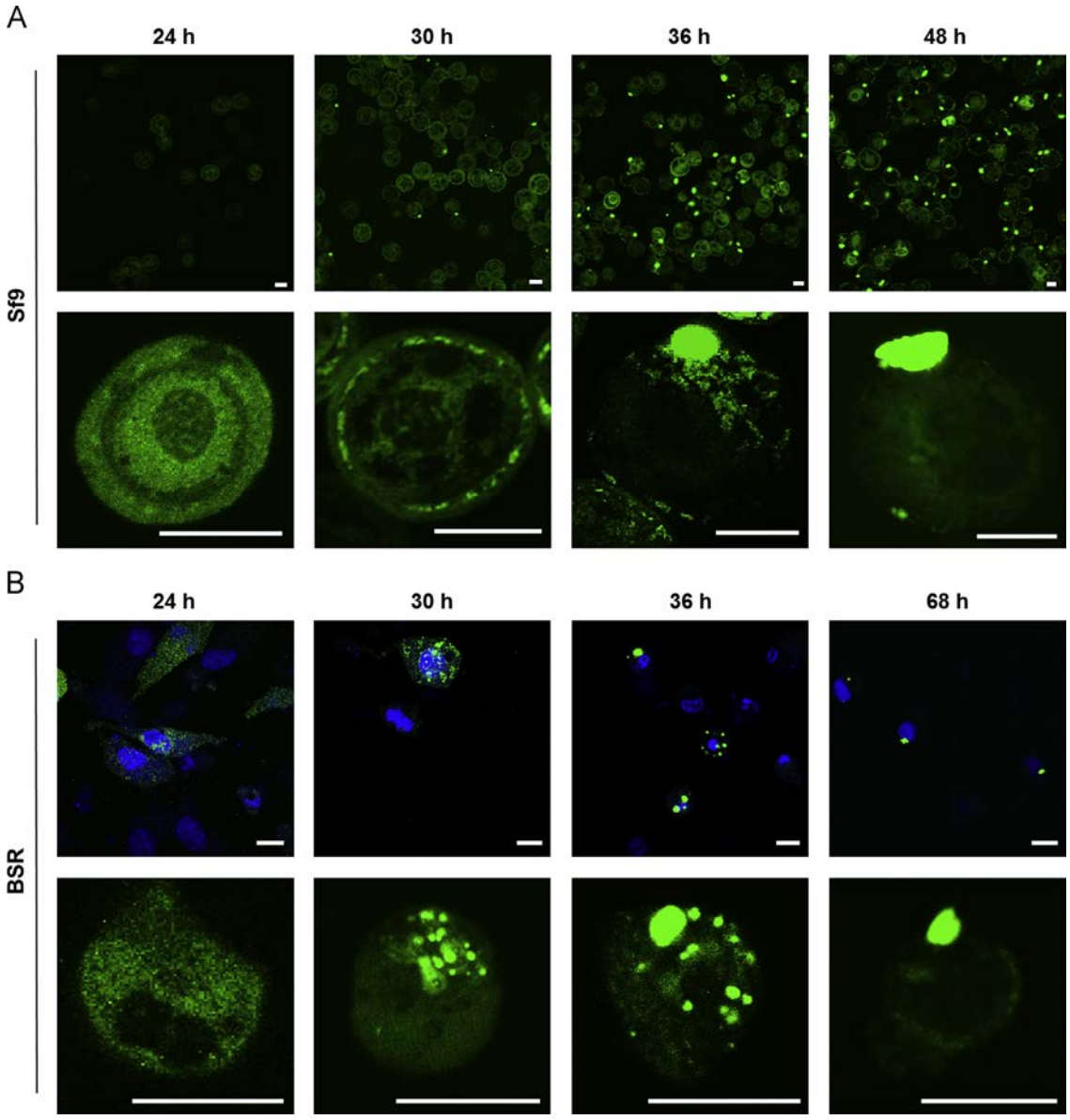

Fig. 5. Intracellular distribution of VP7-144-eGFP fusion protein in recombinant baculovirus-infected Sf9 and transfected BSR cells at indicated times. Sf9 cells (A) and BSR cells (B) expressing VP7-144-eGFP were visualized by confocal microscopy either fixed (top panel) or unfixed (live) (bottom panel) in each case at the indicated times. Nuclei were stained with DAPI (blue). Scale bars represent 10 μm.

(Figs. 8 and 9D) suggesting that VP7 did not use the lysosomal pathway at any stage during VP7 crystalline particle formation.

Discussion

In this study, we have addressed questions associated with the way in which AHSV VP7 is localized in both insect and mammalian cells. We examined the nature of AHSV VP7 crystalline particle formation in order to gain a better understanding of the behaviour of AHSV VP7 during core particle assembly. The protein was found to assemble into distinct flat crystalline-like particles in the presence or absence of other AHSV proteins, and localizes in this fashion independently of the investigated host cellular machinery. Furthermore, the formation of these crystalline-like particles sequesters the majority of VP7 during core assembly. This study offers new insights into the mechanism of AHSV assembly.

The intracellular distribution and trafficking behaviour of a VP7-eGFP fusion protein were examined by immunofluorescence microscopy at various times post infection. We found that VP7 is initially trafficked into numerous foci throughout the cytoplasm. With time, these foci migrate and coalesce to form one or more large crystalline-like particles within the cell. To determine if localization was cell-type specific, experiments were performed in both insect and mammalian cell types. Very similar results were found for both systems, however the large crystalline-like particles of transiently expressed VP7 in mammalian cells were observed at a later time post transfection (68 h p.t.). This delay was most likely due to the lower level of protein expression inherent in transient systems. It has been suggested that crystalline particle formation is a side-effect of AHSV VP7 over-expression in the baculovirus expression system resulting in aggregation of the insoluble protein. Our data illustrates that the formation of VP7 crystalline-like particles is not caused by over-expression, as the transient expression of VP7 in BSR cells as well as VP7 synthesis in AHSV-infected BSR cells yielded VP7 that assembled into crystalline-like particles.

By investigating the interaction of VP7 with cellular trafficking pathways, we showed that VP7 manages to evade the host

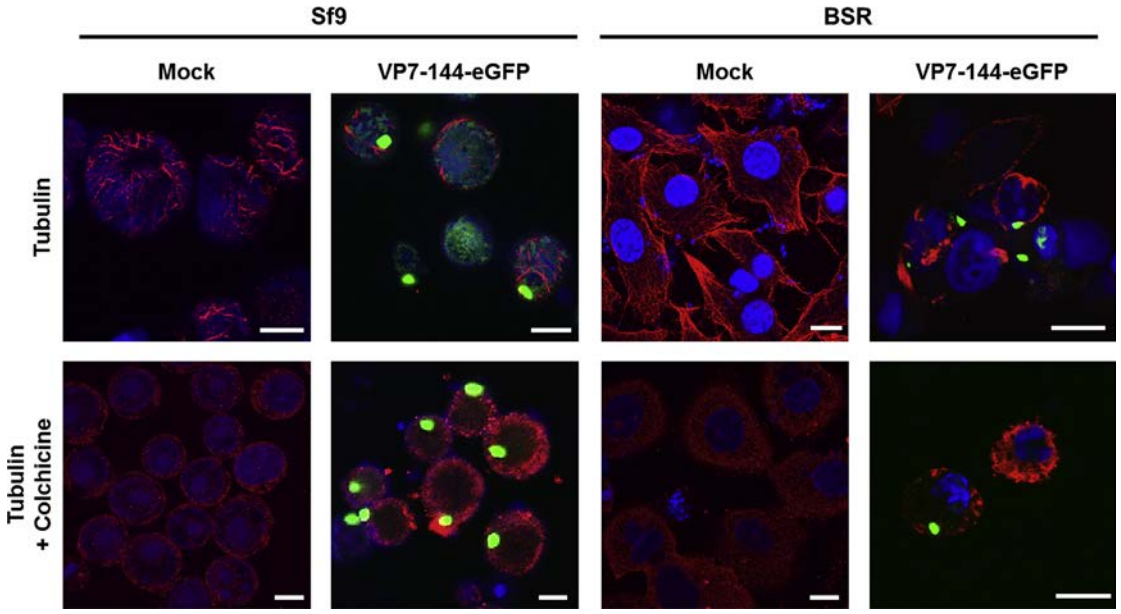

Fig. 6. VP7 is not associated with microtubules in insect and mammalian cells. Sf9 cells were mock infected or infected with recombinant baculovirus expressing VP7-144-eGFP and fixed at 48 h p.i. BSR cell monolayers were mock transfected or transfected with VP7-144-eGFP mammalian expression vector, and fixed at 68 h p.t. Cells were untreated (top panel), or treated with 10 μM colchicine from 0 to 48 h p.i. (Sf9 cells) or 0 to 68 h p.t. (BSR cells) (bottom panel). Cells were immunostained with mouse monoclonal anti-tubulin primary antibody followed by Alexa Fluor 594 conjugated goat anti-mouse IgG (red). VP7-144-eGFP was visualized based on eGFP auto-fluorescence (green). Nuclei were stained with DAPI (blue). Scale bars represent 10 μm.

cell defenses against protein aggregation and crowding. VP7 particle formation was not related to mechanisms of aggresome generation, the ubiquitin–proteasome system, or lysosomal pathways. In addition the results indicate that VP7 crystalline-like particles are not misfolded aggregates, as proteins that are misfolded are typically targeted to the aggresome by histone deacetylase 6. These data imply that VP7 crystalline particle formation is not necessarily a by-product of its innate insolubility and subsequent aggregation, but rather a reflection of a highly ordered process in which VP7 self-assembly takes place during core assembly.

We have shown that VP7 trafficking and crystalline-like particle formation are independent of other AHSV proteins, and of host transport and trafficking machinery investigated here. Thus, the unique trafficking behaviour and the ability of VP7 to form crystalline-like particles are likely to be driven by factors that occur within or are inherent to VP7 itself, i.e. by a process of VP7 self-assembly. Specifically, when VP7 is expressed, it forms trimers in solution (seen by the homogenous distribution of VP7 at the initial stages of expression). These trimers have an inherent affinity for one another through their very strong and very specific side-to-side trimer–trimer interactions (Limn and Roy, 2003). These trimer–trimer interactions are what drive the formation of small foci at the intermediate stages of expression, as well as the coalescence of these foci to form crystalline-like particles at later stages of expression. Capsid proteins of a number of viruses have been shown to self-assemble into a variety of particles or structures (Bancroft et al., 1967; Salunke et al., 1986; Volpers et al., 1994). The capsid protein VP6 of rotavirus has been shown to self-assemble into spherical and helical particles which are dependent on pH conditions, implying that the charge of certain residues within the protein is responsible for self-assembly (Lepault et al., 2001).

It is important to note that it is not trimer formation that drives core assembly, but rather the interactions between trimers that allow VP7 trimers to self-associate and form the VP7 lattice. Limn and Roy (2003) suggest that during core assembly, multiple sheets of BTV VP7 may form at different sites and that lattice formation does not result from trimers loosely associating at one point on VP3. Here we suggest that the VP7 crystalline particles are products of multiple sheets of AHSV VP7 trimers coming together to form highly ordered structures as a result of very strong trimer–trimer interactions in the presence or absence of VP3. Interestingly, BTV VP7 trimers do not form any morphological entities without the presence of VP3 (Kar et al., 2007; Loudon and Roy, 1991); and the formation of a stable BTV VP7 lattice in BTV core assembly requires attachment to the BTV VP3 subcore (Limn and Roy, 2003). This suggests that BTV VP7 trimer–trimer interactions are weaker than those of AHSV VP7 trimers, and AHSV VP7 crystalline-like particle formation appears to be a by-product of inherently strong AHSV VP7 trimer–trimer interactions.

Despite the high level of conservation of VP7 across orbiviruses, it is puzzling that AHSV VP7 behaves in such a unique manner. Viruses are often under selective pressures and genome segments of dsRNA viruses have been shown to evolve independently from one another. Here we show that a large majority of the synthesized VP7 is channelled into these crystalline particles during AHSV assembly. Given the negative effects of aggregation into particles with regards to core assembly and replication rate, it is unclear why the virus would retain this seemingly undesirable feature. To speculate, the crystalline particles may contribute to virus pathogenesis as formation of these crystalline particles could be detrimental to cellular function and membrane integrity. Nonetheless, it is unclear whether VP7 aggregation into these particles is to the benefit or detriment to the virus. Here we show that the formation of crystalline particles is driven by factors inherent to the VP7 protein itself. The next step will be to determine what properties of VP7 drive self-assembly, and to examine the role of VP7 self-assembly in core formation and virus replication. To address this topic, we have used a bioinformatics approach to identify VP7 residues that are responsible for trimer–trimer interactions. By targeting these residues for mutation, we will be able to establish the role of AHSV trimer–trimer interactions in VP7 crystalline particle formation and through a reverse genetics approach we will be able to ascertain the role of crystalline particles in virus replication.

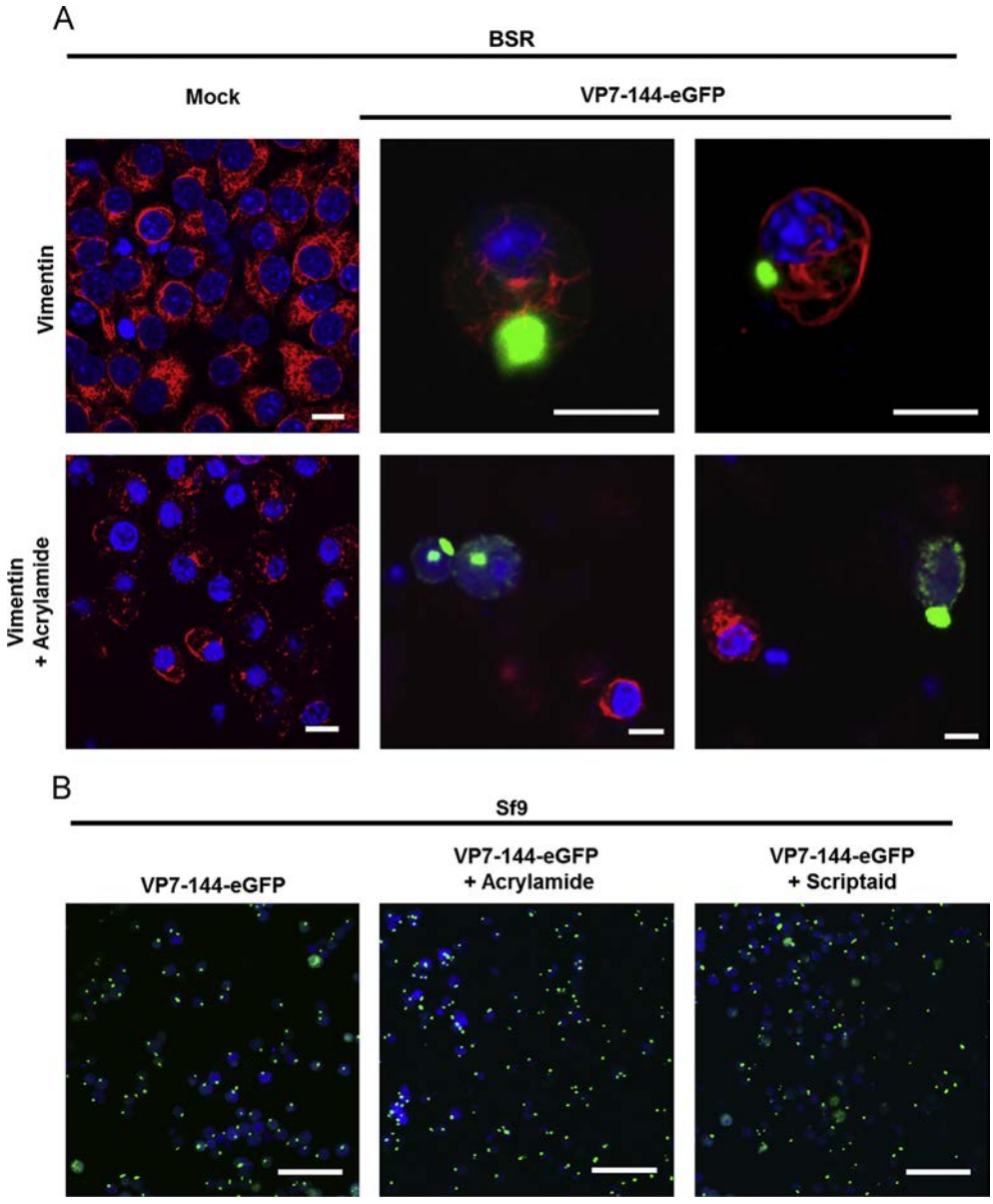

Fig. 7. VP7 is not associated with the aggresomal pathway. (A) BSR monolayers were mock transfected or transfected with VP7-144-GFP mammalian expression vector and incubated in the absence (top panel) or presence (bottom panel) of 5 mM acrylamide. Acrylamide (5 mM) was added to medium 24 h prior to fixation. Cells were fixed at 68 h p.t. and vimentin was stained with mouse monoclonal antibody against vimentin followed by Alexa Fluor 594 conjugated goat anti-mouse IgG (red). VP7-144-eGFP was visualized based on GFP auto-fluorescence (green). Nuclei were stained with DAPI (blue). (B) Sf9 cells were infected with recombinant baculovirus expressing VP7-144-eGFP and incubated in the presence of 5 mM acrylamide or 5 μM Scriptaid from 0 to 48 h p.i. VP7-144-eGFP was visualized based on GFP auto-fluorescence (green). Nuclei were stained with DAPI (blue). Scale bars represent 10 μm in (A) and 100 μm in (B).

We have demonstrated that VP7, although inherently present in high abundance when expressed intracellularly, manages to evade host cell defenses against protein aggregation, over-expression, and presence of foreign protein. During the first stages of replication the newly released core protects the viral genome and enzymes within from host defenses. Furthermore, the addition of VP7 onto the subcore during core assembly may be necessary prior to the trafficking of the core out of VIBs (Matsuo and Roy, 2013). These putative roles of core protein VP7 may offer an explanation for its ability to evade host defenses and it would therefore be expected that VP7, which forms the outer layer of the core particle, possesses the ability to remain a highly stable outer core layer capable of protecting the subcore within from host cell defenses against invasion.

Materials and methods

Cells and viruses

Spodoptera frugiperda (Sf9) cells were maintained at 27 °C in suspension or monolayer cultures in TC-100 insect medium (Sigma) with nonessential amino acids (Highveld Biological) supplemented with 10% fetal calf serum (FCS) and the appropriate antibiotics (penicillin, streptomycin, and fungizone). Recombinant baculoviruses were generated using the Bac-to-Bac Baculovirus expression system (Life Technologies) and were propagated in Sf9 cells. Recombinant plaque-purified baculoviruses, capable of expressing wild-type AHSV-9 VP7; wild-type AHSV-9 VP3; wild-type AHSV-9 NS2; and eGFP in Sf9 cells were available at the start

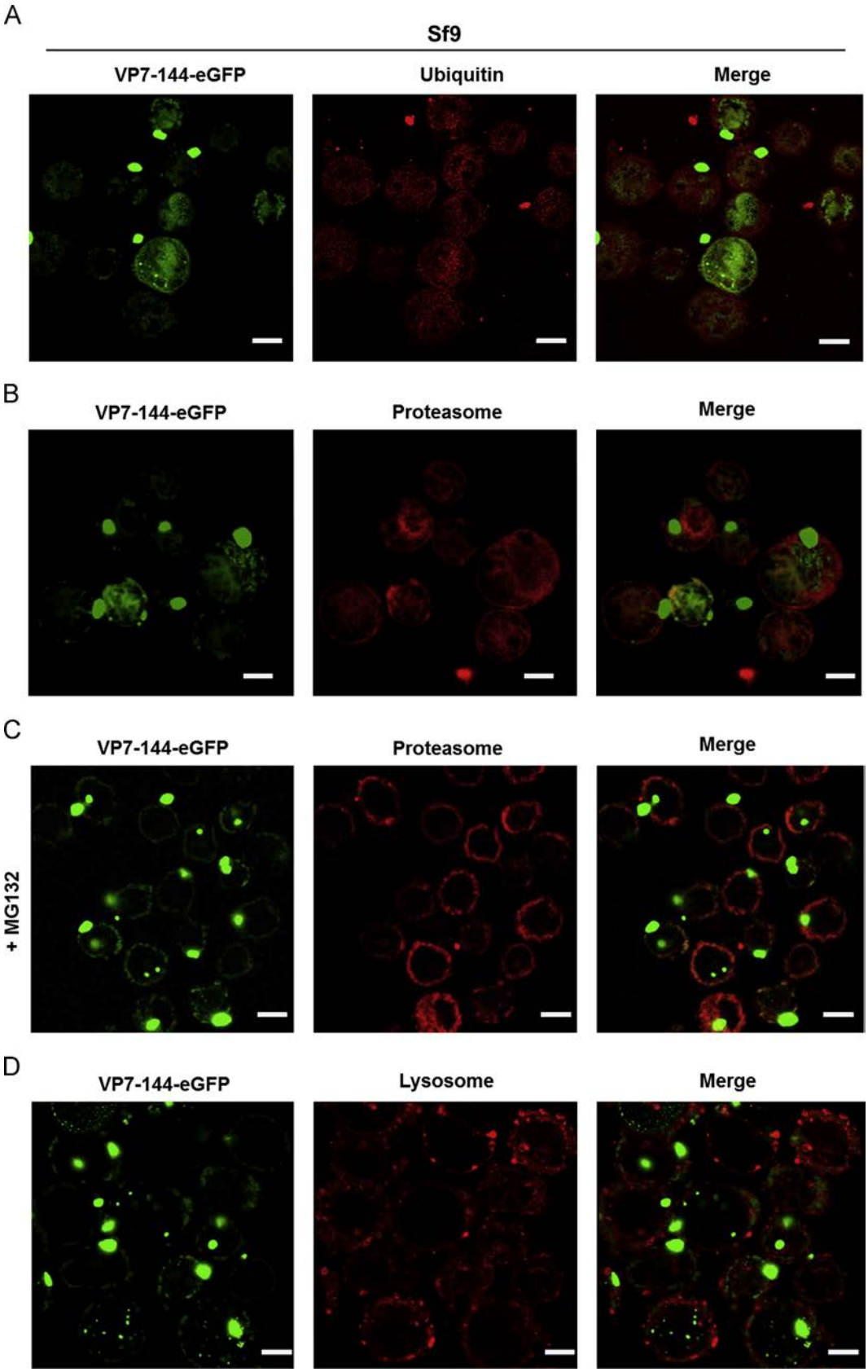

Fig. 8. VP7 is not associated with the ubiquitin–proteasome system or the lysosomal pathway in insect cells. Sf9 cells were infected with recombinant baculovirus expressing VP7-144-eGFP, fixed at 48 h p.i., and labeled using antibodies against ubiquitin (mouse) (A) or the 26 S proteasome (rabbit) (B) followed by Alexa Fluor 594 conjugated goat anti-mouse IgG or Alexa Fluor 633 conjugated goat anti-rabbit IgG (red) respectively. To inhibit the proteasome, cells expressing VP7-144-eGFP were incubated in the presence of 100 μM MG132 24 h prior to fixation followed by the staining of the 26 S proteasome (C). Lysosomes were labeled using Lysotracker Red Dye (Life Technologies) (D). Scale bars represent 10 μm.

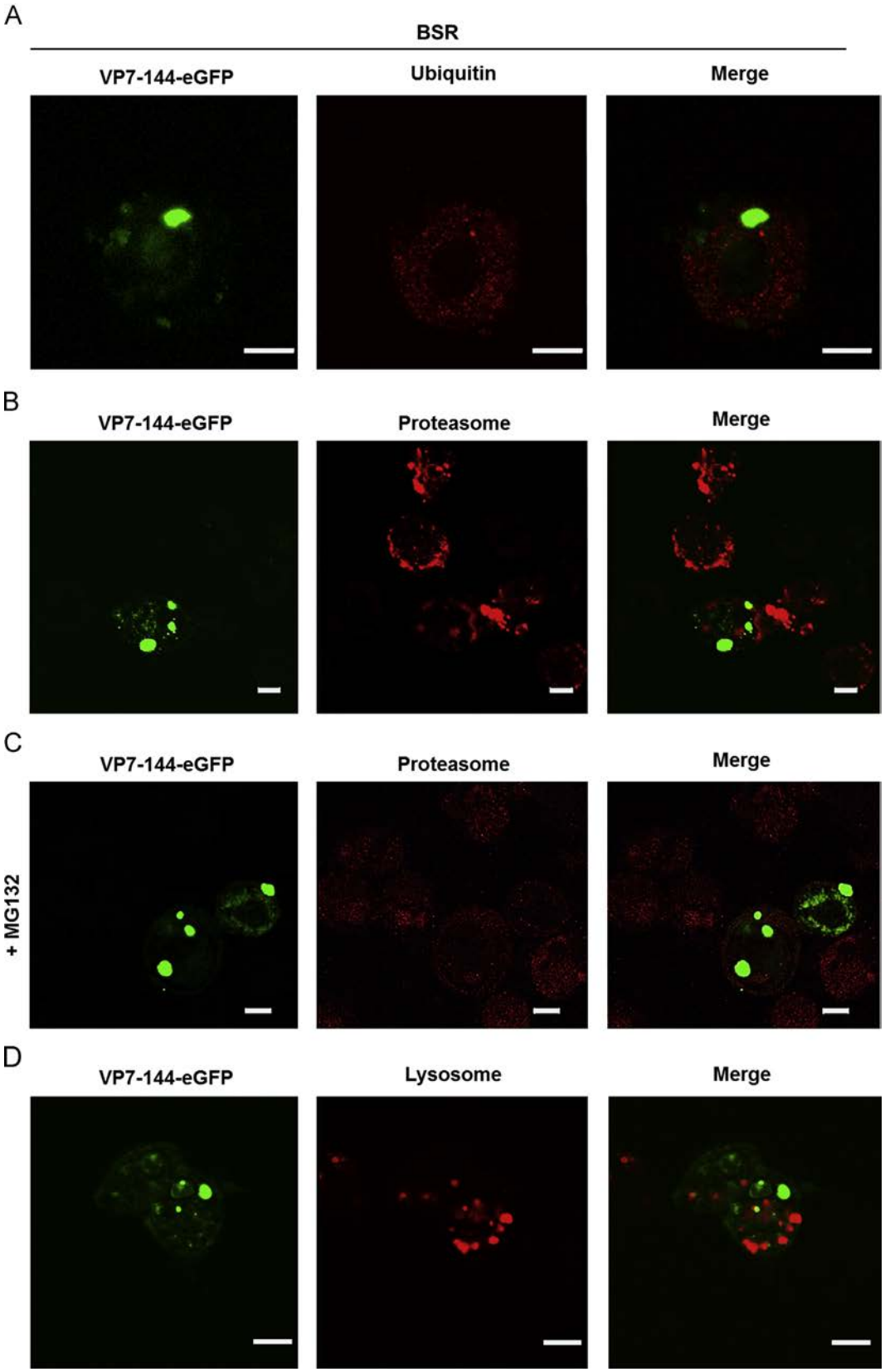

Fig. 9. VP7 is not associated with the ubiquitin–proteasome system or the lysosomal pathway in mammalian cells. BSR cells were transfected with VP7-144-eGFP mammalian expression vector and fixed at 68 h p.t. Cells were labeled with antibodies against ubiquitin (mouse) (A) or the 26 S proteasome (rabbit) (B) followed by Alexa Fluor 594 conjugated goat anti-mouse IgG or Alexa Fluor 633 conjugated goat anti-rabbit IgG (red) respectively. To inhibit the 26 S proteasome, transfected cells were incubated in the presence of 100 μM MG132 24 h prior to fixation followed by the staining of the 26 S proteasome (C). Lysosomes were labeled using LysoTracker Red Dye (Life Technologies) (D). Scale bars represent 5 μm.

of the experiment (Maree et al., 1998; Rutkowska et al., 2011; Uitenweerde et al., 1995). BSR cells, a derivative of baby hamster kidney (BHK) cells, were maintained in monolayers in Minimal Essential Medium (MEM) with nonessential amino acids (Highveld Biological) supplemented with 5% FCS and antibiotics (penicillin, streptomycin, and fungizone) (Highveld Biological) at 37 °C in the presence of 5% CO_2. AHSV-4 was propagated in BHK cells and the titre was determined by plaque assay in BSR cells.

Construction of pFb-VP7-144-eGFP and generation of recombinant baculovirus for expression in insect cells

To construct a VP7-eGFP fusion protein, we inserted the eGFP gene into the EcoRI and XhoI restriction endonuclease (R. E.) sites of a previously constructed modified AHSV-9 VP7 vector, pFb-VP7-144(P_2) (Rutkowska et al., 2011). The pFb-VP7-144(P_2) vector is a pFastbac 1 plasmid that contains a modified AHSV-9 VP7 gene with an insertion of 18 nucleotides comprising R. E. recognition sites for SmaI, EcoRI, and XhoI at position 431-432 which results in a peptide insertion of PGEFLE downstream of amino acid position 144 in the AHSV-9 VP7 top domain. To insert the eGFP gene at the 144 amino acid site, primers that were flanked with EcoRI (forward) and XhoI (reverse) R. E. sites were used to amplify the eGFP gene from a pGEM-Teasy-eGFP plasmid (supplied by Prof. J. Theron, University of Pretoria, Department of Microbiology). The pFb-VP7-144(P_2) vector was simultaneously digested with EcoRI and XhoI restriction endonucleases, and the eGFP amplicon was inserted by directional cloning. Recombinant baculoviruses were generated as described previously (Rutkowska et al., 2011).

SDS-polyacrylamide gel electrophoresis (SDS-PAGE) and Western blot analysis

Sf9 monolayers were infected with recombinant baculovirus using a multiplicity of infection (MOI) of 5–10 and incubated at 27 °C. Cells were harvested at 48 h post infection, washed with phosphate-buffered saline (PBS), and lysed at 4 °C in lysis buffer (10 mM Tris–HCl [pH 8.0], 50 mM EDTA, 10 mM NaCl, 0.5% [v/v] Nonidet® P-40). Samples were then suspended in 6.6 μl o f 3 × protein dissociation buffer (10% [v/v] β-mercaptoethanol, 4% (w/v) SDS, 20% (v/v) glycerol, 125 mM Tris–HCl [pH 6.8], and 0.002%(w/v) bromophenol blue) and either boiled at 95 °C or incubated at room temperature (for identification of trimers) (Monastyrskaya et al., 1997) for 5 min and resolved by 12% SDS-PAGE, followed by staining with Coomassie brilliant blue. For Western blot analysis, proteins from SDS-PAGE gels were transferred to a Hybond nitrocellulose membrane (Amersham) by standard blotting procedures. Membranes were incubated in buffer with anti-VP7 (guinea pig) primary antibody. Peroxidase-conjugated Protein A (ICN) was used for detection.

Construction of pcDNA™3.2/V5-DEST-VP7-144-eGFP mammalian expression vector for transient expression in mammalian cells

In order to express the VP7-144-eGFP fusion protein in mammalian cells, the polymerase chain reaction (PCR) was used to amplify the full-length VP7-144-eGFP gene from the pFb-VP7-144-eGFP plasmid. The PCR product was adenylated and subcloned (using TA cloning) in pCR®8/GW/TOPO® entry vector (Life Technologies) according to the manufacturer's instructions. The VP7-144-eGFP gene was then recombined into the mammalian expression vector, pcDNA™3.2/V5-DEST (Life Technologies) by means of LR recombination (Gateway®). The authenticity of each construct was confirmed by DNA sequencing. The mammalian expression vector, pcDNA™3.2/V5-DEST-VP7-144-eGFP was used for transient VP7-144-eGFP expression in BSR cells.

Transfection of BSR cells

For the transient expression of VP7-144-eGFP in mammalian cells, 2.2×10^5 cells were seeded the day before transfection in 24-well plates (2 cm^2 per well) containing 8 mm round glass coverslips. A total of 0.8 μg of pcDNA™3.2/V5-DEST-VP7-144-GFP vector DNA was transfected into BSR cells using 2 μl of Lipofectamine2000 (Life Technologies) in serum-free MEM as suggested by the manufacturer. Transfected cells were incubated at 37 °C for 12–68 h depending on the experiment. Protein expression was examined and confirmed based on eGFP auto-fluorescence using a Zeis LSM 510 Meta confocal microscope.

Antibodies and pharmacological reagents

Primary antibody against AHSV-4 VP7 (guinea pig) and NS2 (rabbit) were available at the start of this investigation (Rutkowska et al., 2011; Uitenweerde et al., 1995). Mouse monoclonal primary antibodies against β-tubulin (clone TUB 2.1), vimentin (clone V9) as well as the IgG conjugated to FITC (anti-guinea pig) secondary antibody were obtained from Sigma. Mouse monoclonal primary antibody against ubiquitin (clone Ubi-1) and rabbit polyclonal antibody against 26 S proteasome were obtained from Thermo Scientific. LysoTracker Red Dye and IgG conjugated to Alexa Fluor 594 (mouse) or Alexa Fluor 633 (rabbit) were purchased from Molecular Probes (Life Technologies). DAPI (4′,6-Diamidine-2′-phenylindole dihydrochloride) was purchased from Roche. For pharmacological experiments, colchicine, acrylamide, MG132, and Scriptaid were obtained from Sigma.

Immunofluorescence microscopy

Cell monolayers were grown on sterile glass coverslips in 24-well plates. Sf9 monolayers were infected with recombinant baculovirus at a MOI of 10 and incubated at 27 °C for 24–48 h before being fixed in a 1:1 methanol:acetone solution at 4 °C for 5 min. BSR monolayers were transfected with plasmid DNA as described above, and incubated at 37 °C for 48–68 h and fixed for 30 min at room temperature with 4% (w/v) paraformaldehyde (PFA) in PBS. Cover slips were then incubated for 15 min at room temperature with 0.5% Triton X-100 in PBS to permeabilize the cells. For labeling experiments, Sf9 and BSR cells were blocked in 5% blocking solution (5% milk powder in PBS) directly after fixation followed by incubation with primary antibodies for 1 h. The cells were washed three times with wash buffer (0.5% (v/v) Tween20 in PBS) and incubated for 1 h with appropriate second-ary antibodies conjugated to FITC (green), Alexa Fluor 594 (red), or Alexa Fluor 633 (red). Cells were washed again (as above) and stained with 10 μg/ml DAPI in 1% blocking solution for 10 min. For direct immunofluorescence experiments, cells were stained with DAPI directly after fixation. Cells were washed once with PBS before being mounted onto glass slides using VECTASHIELD Mounting Medium (Vector Laboratories). Slides were then viewed using a Zeiss LSM 510 Meta confocal microscope and images were obtained using Zeiss LSM Image Browser Version 4.2.0.121.

Treatment of Sf9 and BSR cells with transport inhibitors

Sf9 cells were infected with recombinant baculovirus at MOI of 10 or BSR cells were transfected as described above. Fresh medium containing either 10 μM colchicine, 5 mM acrylamide, 100 μM MG132, or 5 μM scriptaid was added to the cells at indicated times post infection or transfection. After incubation, cells were fixed and processed for immunofluorescence as described above.

Acknowledgments

This work was supported by BioPad Bric Grant BP050 and the Poliomyelitis Research Foundation, South Africa Grant 10/12. Graduate bursary support was received from the National Research Foundation, South Africa and University of Pretoria, South Africa. We thank Flip Wege for technical support with cell culture and Tumelo Seameco for his role in the construction of the recombinant baculovirus expressing VP7-144-eGFP. We also appreciate the support from both Alan Hall from the Laboratory for Microscopy & Microanalysis at the University of Pretoria and Soné Ungerer for their support with confocal microscopy.

References

Bancroft, J.B., Hills, G.J., Markham, R., 1967. A study of the self-assembly process in a small spherical virus formation of organized structures from protein subunits in vitro. Virology 31, 354–379.

Basak, A.K., Gouet, P., Grimes, J., Roy, P., Stuart, D., 1996. Crystal structure of the top domain of African horse sickness virus VP7: comparisons with bluetongue virus VP7. J. Virol. 70, 3797–3806.

Basak, A.K., Stuart, D.I., Roy, P., 1992. Preliminary crystallographic study of bluetongue virus capsid protein, VP7. J. Mol. Biol. 228, 687–689.

Beaudoin, S., Goggin, K., Bissonnette, C., Grenier, C., Roucou, X., 2008. Aggresomes do not represent a general cellular response to protein misfolding in mammalian cells. BMC Cell Biol. 9, 59.

Bhattacharya, B., Noad, R.J., Roy, P., 2007. Interaction between Bluetongue virus outer capsid protein VP2 and vimentin is necessary for virus egress. Virol. J. 4, 7.

Brookes, S.M., Hyatt, A.D., Eaton, B.T., 1993. Characterization of virus inclusion bodies in bluetongue virus-infected cells. J. Gen. Virol. 74 (Pt 3), 525–530.

Burroughs, J.N., O'Hara, R.S., Smale, C.J., et al., 1994. Purification and properties of virus particles, infectious subviral particles, cores and VP7 crystals of African horsesickness virus serotype 9. J. Gen. Virol. 75 (Pt 8), 1849–1857.

Chuma, T., Le Blois, H., Sanchez-Vizcaino, J.M., Diaz-Laviada, M., Roy, P., 1992. Expression of the major core antigen VP7 of African horsesickness virus by a recombinant baculovirus and its use as a group-specific diagnostic reagent. J. Gen. Virol. 73 (Pt 4), 925–931.

Ciechanover, A., 2005. Proteolysis: from the lysosome to ubiquitin and the proteasome. Nat Rev Mol Cell Biol 6, 79–87.

Dohner, K., Nagel, C.H., Sodeik, B., 2005. Viral stop-and-go along microtubules: taking a ride with dynein and kinesins. Trends Microbiol. 13, 320–327.

Du Toit, R.M., 1944. The transmission of bluetongue and horsesickness by Culicoides. Onderstepoort J. Vet. Sci. Anim. Ind. 19, 7–16.

French, T.J., Roy, P., 1990. Synthesis of bluetongue virus (BTV) corelike particles by a recombinant baculovirus expressing the two major structural core proteins of BTV. J. Virol. 64, 1530–1536.

Grimes, J., Basak, A.K., Roy, P., Stuart, D., 1995. The crystal structure of bluetongue virus VP7. Nature 373, 167–170.

Grimes, J.M., Burroughs, J.N., Gouet, P., et al., 1998. The atomic structure of the bluetongue virus core. Nature 395, 470–478.

Grimes, J.M., Jakana, J., Ghosh, M., et al., 1997. An atomic model of the outer layer of the bluetongue virus core derived from X-ray crystallography and electron cryomicroscopy. Structure 5, 885–893.

Grubman, M.J., Lewis, S.A., 1992. Identification and characterization of the structural and nonstructural proteins of African horsesickness virus and determina-tion of the genome coding assignments. Virology 186, 444–451.

Hassan, S.H., Wirblich, C., Forzan, M., Roy, P., 2001. Expression and functional characterization of bluetongue virus VP5 protein: role in cellular permeabilization. J. Virol. 75, 8356–8367.

Hassan, S.S., Roy, P., 1999. Expression and functional characterization of blue tonguevirus VP2 protein: role in cell entry. J. Virol. 73, 9832–9842.

Heath, C.M., Windsor, M., Wileman, T., 2001. Aggresomes resemble sites specialized for virus assembly. J. Cell Biol. 153, 449–456.

Hewat, E.A., Booth, T.F., Loudon, P.T., Roy, P., 1992a. Three-dimensional reconstruction of baculovirus expressed bluetongue virus core-like particles by electron microscopy. Virology 189, 10–20.

Hewat, E.A., Booth, T.F., Roy, P., 1992b. Structure of bluetongue virus particles by cryoelectron microscopy. J. Struct. Biol. 109, 61–69.

Huismans, H., van Dijk, A.A., Els, H.J., 1987. Uncoating of parental bluetongue virus to core and subcore particles in infected L cells. Virology 157, 180–188.

Huismans, H., Verwoerd, D.W., 1973. Control of transcription during the expression of the bluetongue virus genome. Virology 52, 81–88.

Kar, A.K., Bhattacharya, B., Roy, P., 2007. Bluetongue virus RNA binding protein NS2is a modulator of viral replication and assembly. BMC Mol. Biol. 8, 4.

Kawaguchi, Y., Kovacs, J.J., McLaurin, A., et al., 2003. The deacetylase HDAC6 regulates aggresome formation and cell viability in response to misfolded protein stress. Cell 115, 727–738.

Kopito, R.R., 2000. Aggresomes, inclusion bodies and protein aggregation. Trends Cell Biol. 10, 524–530.

Le Blois, H., Roy, P., 1993. A single point mutation in the VP7 major core protein of bluetongue virus prevents the formation of core-like particles. J. Virol. 67, 353–359.

Lepault, J., Petitpas, I., Erk, I., et al., 2001. Structural polymorphism of the major capsid protein of rotavirus. EMBO J. 20, 1498–1507.

Limn, C.K., Roy, P., 2003. Intermolecular interactions in a two-layered viral capsid that requires a complex symmetry mismatch. J. Virol. 77, 11114–11124. Limn, C.K., Staeuber, N., Monastyrskaya, K., Gouet, P., Roy, P., 2000. Functional dissection of the major structural protein of bluetongue virus: identification of key residues within VP7 essential for capsid assembly. J. Virol. 74, 8658–8669.

Loudon, P.T., Roy, P., 1991. Assembly of five bluetongue virus proteins expressed by recombinant baculoviruses: inclusion of the largest protein VP1 in the core and virus-like proteins. Virology 180, 798–802.

Maree, S., Durbach, S., Huismans, H., 1998. Intracellular production of African horsesickness virus core-like particles by expression of the two major core proteins, VP3 and VP7, in insect cells. J. Gen. Virol. 79 (Pt 2), 333–337.

Matsuo, E., Roy, P., 2013. Minimum requirements for bluetongue virus primary replication in vivo. J. Virol. 87, 882–889.

Mellor, P.S., Hamblin, C., 2004. African horse sickness. Vet. Res. 35, 445–466.

Monastyrskaya, K., Staeuber, N., Sutton, G., Roy, P., 1997. Effects of doma in-switching and site-directed mutagenesis on the properties and functions of the VP7 proteins of two orbiviruses. Virology 237, 217–227.

Moshe, A., Gorovits, R., 2012. Virus-induced aggregates in infected cells. Viruses 4, 2218–2232.

Oldfield, S., Adachi, A., Urakawa, T., Hirasawa, T., Roy, P., 1990. Purification and characterization of the major group-specific core antigen VP7 of bluetongue virus synthesized by a recombinant baculovirus. J. Gen. Virol. 71, 2649.

Prasad, B.V., Yamaguchi, S., Roy, P., 1992. Three-dimensional structure of single-shelled bluetongue virus. J. Virol. 66, 2135–2142.

Roy, P., Hirasawa, T., Fernandez, M., Blinov, V.M., Sanchez-Vixcain Rodrique, J.M., 1991. The complete sequence of the group-specific antigen, VP7, of African horsesickness disease virus serotype 4 reveals a close relationship to bluetongue virus. J. Gen. Virol. 72 (Pt 6), 1237–1241.

Roy, P., Mertens, P.P., Casal, I., 1994. African horse sickness virus structure. Comp. Immunol. Microbiol. Infect. Dis. 17, 243–273.

Rutkowska, D.A., Meyer, Q.C., Maree, F., et al., 2011. The use of soluble African horsesickness viral protein 7 as an antigen delivery and presentation system. Virus Res. 156, 35–48.

Salunke, D.M., Caspar, D.L.D., Garcea, R.L., 1986. Self-assembly of purified polyomavirus capsid protein VP1. Cell 46, 895–904.

Uitenweerde, J.M., Theron, J., Stoltz, M.A., Huismans, H., 1995. The multimeric nonstructural NS2 proteins of bluetongue virus, African horsesickness virus, and epizootic hemorrhagic disease virus differ in their single-stranded RNA-binding ability. Virology 209, 624–632.

Venter, E., van der Merwe, C.F., Buys, A.V., Huismans, H., van Staden, V., 2014. Comparative ultrastructural characterization of African horse sickness virus-infected mammalian and insect cells reveals a novel potential virus release mechanism from insect cells. J. Gen. Virol. 95, 642–651.

Venter, E., van der Merwe, C.F., Van Staden, V., 2012. Utilization of cellulose microcapillary tubes as a model system for culturing and viral infection of mammalian cells. Microsc. Res. Tech. 75, 1452–1459.

Venter, G.J., Wright, I.M., Van Der Linde, T.C., Paweska, J.T., 2009. The oralsusceptibility of South African field populations of Culicoides to African horse sickness virus. Med. Vet. Entomol. 23, 367–378.

Vogel, F., Hofius, D., Sonnewald, U., 2007. Intracellular trafficking of potato leafroll virusmovement protein in transgenic arabidopsis. Traffic 8, 1205–1214. Volpers, C., Schirmacher, P., Streeck, R.E., Sapp, M., 1994. Assembly of the major and the minor capsid protein of human papillomavirus type 33 into virus-like particles and tubular structures in insect cells. Virology 200, 504–512.

Wileman, T., 2006. Aggresomes and autophagy generate sites for virus replication. Science 312, 875–878.

Wileman, T., 2007. Aggresomes and pericentriolar sites of virus assembly: cellular defense or viral design? Annu. Rev. Microbiol. 61, 149–167.